Journal of the European Ceramic Society **6** (1990) 351–359

Microstructure and Phase Development in $NiMn_2O_4$ Spinel Ceramics During Isothermal Sintering

J. Jung,[a] J. Töpfer,[a] J. Mürbe[b] & A. Feltz[a]

[a] Friedrich-Schiller University, Department of Chemistry, A.-Bebel-Str. 2, Jena 6900, GDR
[b] Keramische Werke Hermsdorf, Hermsdorf 6530, GDR

(Received 9 April 1990; accepted 22 June 1990)

Abstract

Studies of the sintering behaviour of $NiMn_2O_4$ semiconducting ceramics at 1100°C under oxygen atmosphere show the advantage of a powder prepared by thermal decomposition of oxalate mixed crystals $NiMn_2(C_2O_4)_3 . 6H_2O$ at 450°C for the formation of dense ceramics with homogeneous microstructure. The microstructure of the semiconductor ceramics was established by image analysis. SEM and EDX indicate a phase separation related to partial oxygen loss as observed by thermogravimetry and redox analytic measurements. Reoxidation to a single-phase homogeneous microstructure by annealing at 800°C is possible only in porous samples. $NiMn_2O_4$ is not stable in oxygen at 1100°C. The spinel decomposes into NiO and a Mn-rich spinel matrix $Ni_x^{II}Mn_{1-x}^{II}Mn_2^{III}O_4$. For producing a reproducible semiconducting ceramics it is necessary to stimulate sintering by separation of NiO. A one-phase spinel is obtained by reoxidation of long duration.

Die Sinterstudien zur Herstellung von $NiMn_2O_4$ Halbleiterkeramik bei 1100°C unter Sauerstoffatmosphäre zeigen den Vorteil eines durch Zersetzung von Oxalatmischkristallen $NiMn_2(C_2O_4)_3 . 6H_2O$ bei 450°C erhaltenen Pulvers bezüglich der Ausbildung eines einheitlichen dichten Keramikgefüges, was durch Bildanalyse belegt wird. SEM und EDX lassen eine Phasenausscheidung erkennen, die nach thermogravimetrischen und redox analytischen Untersuchungen mit einer partiellen Sauerstoffabspaltung verbunden ist und durch Halten bei 800°C nur bei hinreichend porösen Proben unter Rückbildung eines einphasigen homogenen Keramikgefüges reversibel ist. $NiMn_2O_4$ ist bei 1100°C in reinem Sauerstoff nicht stabil. An Luft erfolgt Zerfall in NiO und Bildung einer Mn-reicheren $Ni_x^{II}Mn_{1-x}^{II}Mn_2^{III}O_4$ Spinellmatrixphase. Für die Herstellung einer reproduzierbaren Halbleiterkeramik ist es sinnvoll, durch NiO-Ausscheidung die Sinterung zu stimulieren. Der einphasige Spinell wird durch Langzeit-Rückoxydation erhalten.

L'étude du frittage de céramiques semi-conductrices $NiMn_2O_4$ à 1100°C sous oxygène montre les avantages apportés par l'utilisation d'une poudre préparée par décomposition thermique à 450°C de cristaux mixtes d'oxalate $NiMn_2(C_2O_4)_3 . 6H_2O$ pour l'obtention de céramiques denses à microstructure homogène. On a caractérisé la microstructure de ces céramiques par analyse d'image. Les analyses MEB et EDS révèlent une séparation de phases que l'on peut relier à la perte partielle d'oxygène mise en évidence par les mesures thermogravimétriques et redox. La réoxydation en une microstructure homogène monophasée par recuit à 800°C n'est possible que pour des échantillons poreux. $NiMn_2O_4$ n'est pas stable à 1100°C dans l'oxygène. Le spinelle se décompose en NiO et en une matrice spinelle $Ni_x^{II}Mn_{1-x}^{II}Mn_2^{III}O_4$ riche en Mn. L'activation du frittage par séparation de NiO est nécessaire pour élaborer de manière reproductible des céramiques semi-conductrices. Un spinelle monophasé est obtenu par une longue durée de réoxydation.

1 Introduction

Ni–Mn spinels are important as semiconductor ceramic materials. The phase relations were investigated in 1964 by Wickham.[1] Recently the formation of defect spinels after thermal decomposition

Journal of the European Ceramic Society 0955-2219/90/$3.50

of oxalate mixed crystals was described.[2] The advantageous sintering behaviour of defect spinels during heat up was characterized as reaction sintering.[3]

This paper deals with the processing of dense ceramics with a single-phase microstructure. In particular, $NiO.Mn_2O_3$ powder mixtures prepared by thermal decomposition of $NiCO_3$–$MnCO_3$ mixtures (powder A) are compared with metastable defect spinel powders prepared by the thermal decomposition of oxalate mixed crystals $NiMn_2(C_2O_4)_3 \cdot 6H_2O$ (powder B).

2 Materials and Methods

Starting materials were of reagent grade. Mixtures of $NiCO_3$–$MnCO_3$ in the molar ratio 1:2 were thermally decomposed at 600°C for 6 h (powder A). The oxalate mixed crystals ($NiMn_2(C_2O_4)_3.6H_2O$) were decomposed in the temperature range from 350°C to 450°C during 6 h in flowing air[2] (powder B). The promotion of sintering was investigated by the addition of 1 wt% $Pb_5Ge_3O_{11}$, wet-milled with the powder. (Powder mixtures without sintering aid are denoted with the index 0 (A_0, B_0), those with sintering aid with the index 1 (A_1, B_1).) The powders were pressed to tablets 5 mm in diameter and 2 mm thick.[3]

Powder A with 12 m^2/g specific surface area, like powder B with 10 m^2/g specific surface area, was compacted to 50% of the theoretical density. After burn-out of the pressing aid, the samples were sintered in a tube furnace under flowing air or oxygen for four different periods, varying from 1 to 40 h. Figure 1 shows the sintering schedule with 40 h isothermal sintering.

Maximum temperature, time at the maximum temperature, and time of reoxidation at 800°C were varied. The sinter densities of the ceramics were determined by Archimedes' method in heptane. The stoichiometry of the sintered compacts was controlled by the determination of the oxidation

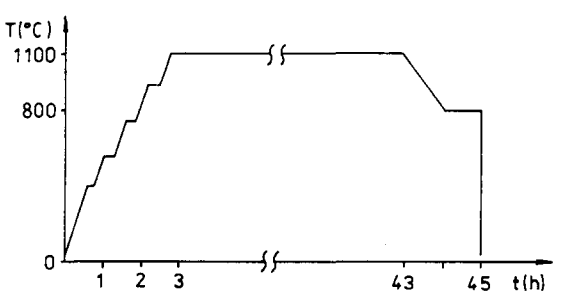

Fig. 1. Sintering schedule of samples for image analysis (40 h sintering time).

equivalents after dissolving the samples in a sulphuric acid solution of VO^{2+} ions.[2]

To assess the phase homogeneity in the volume of the sintered bodies, they were cut in the middle, set in cold hardened epoxy-resin, ground with successively finer abrasive papers, and finally polished with alumina suspension on a cloth. The contrast of the microstructure was best improved by etching with a mixture of HNO_3, CH_3COOH in water (1:1:3) at 80°C for 5–6 minutes. The freshly etched cross-sections were investigated by microscopy (Carl-Zeiss Jena Neophot 21) and photographs were taken. Quantitative image analysis under enlargements of × 500 and × 1000 was done directly from the polished and etched cross-sections (SEM-IPS Kontron). The results are presented as relative distributions of equivalent circle diameters.

The quality of the cross-sections even after electronic picture manipulation (shading correction, edge intensification) did not permit automatic measurements; manual correction of the digitalized pictures was required. A minimum of 2000 grains were measured for each sample. The measured areas were equally distributed along a line. After seven days storage, the prepared cross-sections had aged and were without contrast. New polishing and etching was necessary to reveal the grain structure. A precondition for quantitative image analysis was a dense ceramic (density >95%). Efforts to minimize grain break-out in porous samples by epoxy-resin infiltration remained without success.

The cross-sections were investigated with SEM (ARL microprobe SEMQ) before and after etching. It was confirmed that the etching procedure used did not cause microstructure damage, e.g. selective phase solution. In chosen samples, energy dispersive X-ray fluorescence analysis (Kevex EDX 7000) was performed.

3 Microstructure Development During Isothermal Sintering

Following the phase diagram by Wickham[1] the samples for the investigation of time-dependent grain growth were sintered at 1100°C, the upper temperature of $NiMn_2O_4$ stability in O_2. For reproducible adjustment of the temperature-dependent equilibrium of cation distribution, the samples were held at 800°C for 1 h and then quenched.[4]

For powder compacts from the powders A_1 and B_1, sintering for 1, 4, 8 or 40 h in air or oxygen led to microstructures with densities >95%. Without

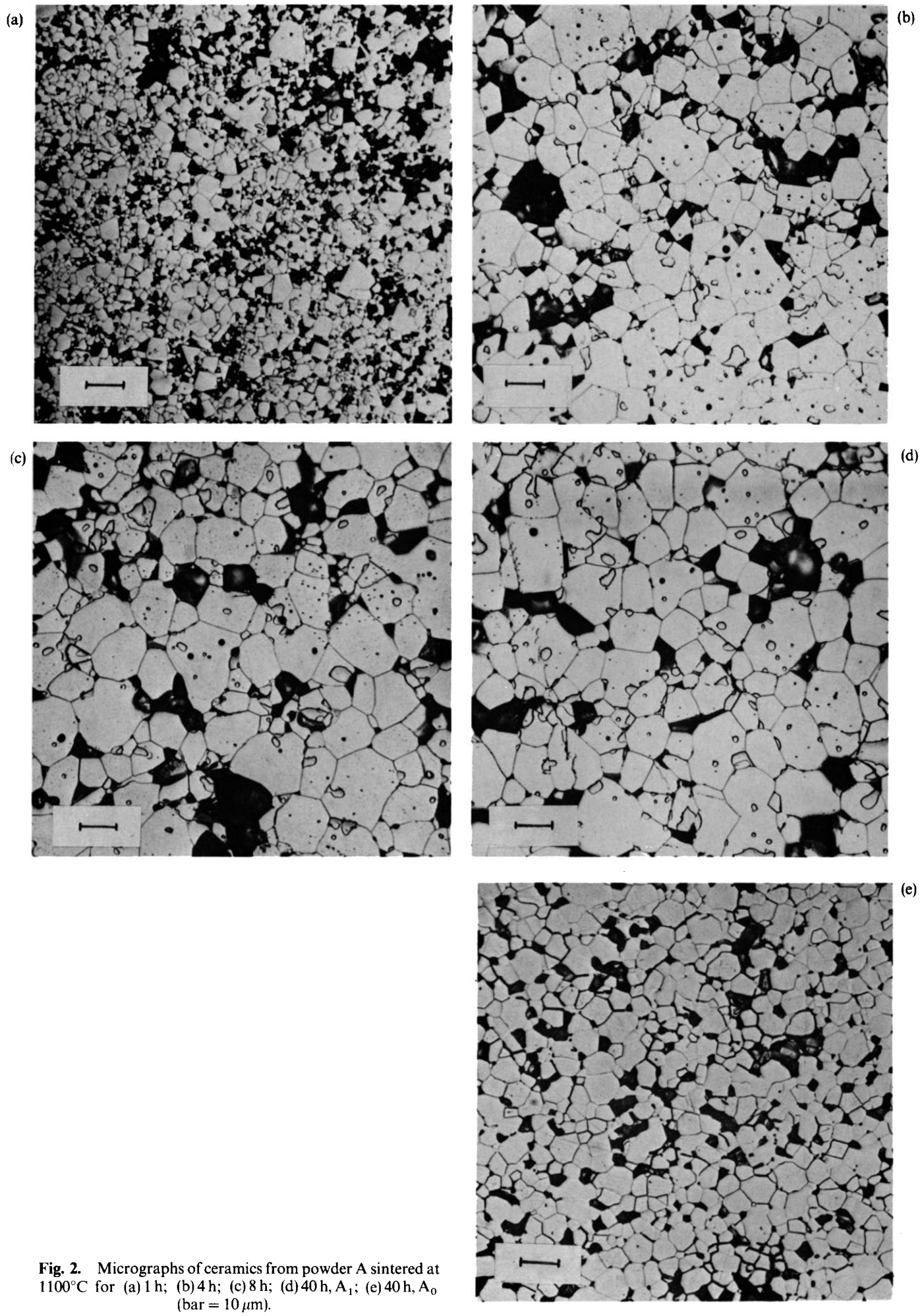

Fig. 2. Micrographs of ceramics from powder A sintered at 1100°C for (a) 1 h; (b) 4 h; (c) 8 h; (d) 40 h, A_1; (e) 40 h, A_0 (bar = 10 μm).

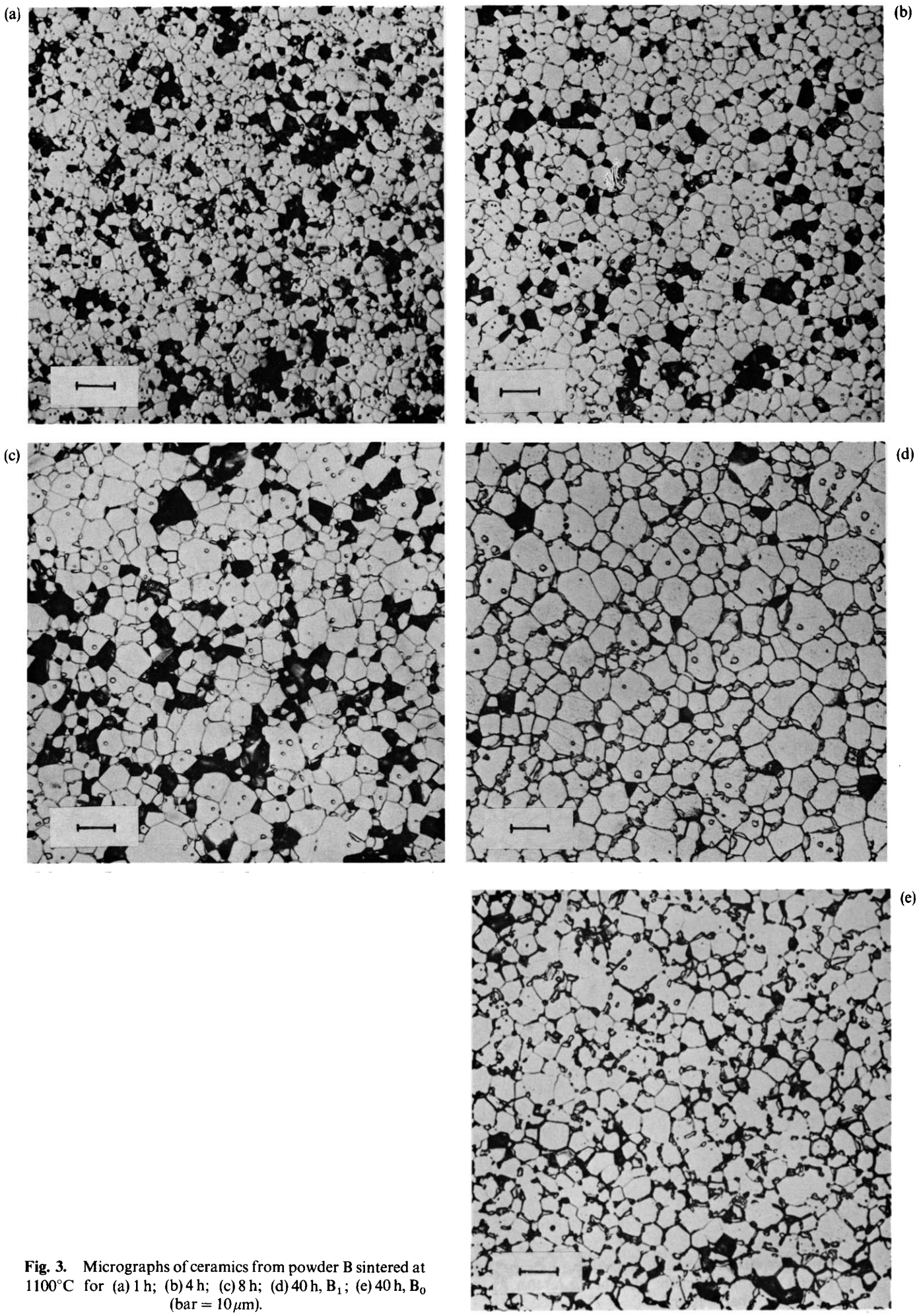

Fig. 3. Micrographs of ceramics from powder B sintered at 1100°C for (a) 1 h; (b) 4 h; (c) 8 h; (d) 40 h, B_1; (e) 40 h, B_0 (bar = 10 μm).

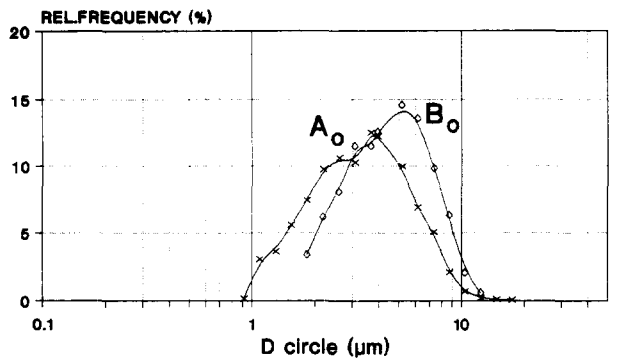

Fig. 4. Grain size distribution in A_0 and B_0 sintered at 1100°C for 40 (see Figs 2(e) and 3(e)).

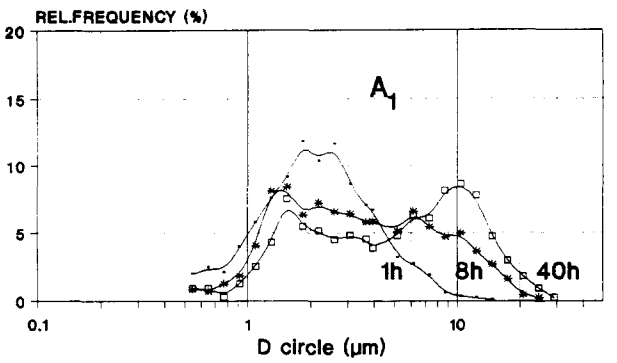

Fig. 6. Development of grain size distribution for ceramics A_1 sintered at 1100°C for 1 h, 8 h and 40 h (see Fig. 2(a), (c) and (d)).

sintering aids, high densities were guaranteed only after 40 h sintering. The micrographs in Figs 2 and 3 show the cross-sections investigated with image analysis. The series of sintering-time increases for ceramics A_1 (Fig. 2(a)–(d)) and B_1 (Fig. 3(a)–(d)) are compared with ceramics A_0 (Fig. 2(e)) and B_0 (Fig. 3(e)) sintered for 40 h. The firings were in O_2 at 1100°C. Essential results are:

—Grain growth, is accelerated by the sintering aid.
—Ceramics made from powder B shows smaller grains and a more homogeneous microstructure.
—With the exception of sample A_0 after 40 h sintering (Fig. 2(e)) all compacts show isolated islands of secondary phase.

The grain size distribution of the samples is shown in Figs 4–7. In Fig. 4 it is surprising that the powder B, in this series with 36 m^2/g specific surface area and without sintering aid, sinters to a slightly coarser microstructure than that of powder A with 12 m^2/g specific surface area. In Fig. 5 it is obvious that under the influence of the melting of the sintering aid in powder A inhomogeneous grain growth to bimodal grain size distribution appears. In contrast to this, the metastable defect spinel powder B prepared by decomposition of oxalate mixed crystals shows lower grain growth to normal grain size distribution.

This finding is confirmed by Figs 6 and 7, demonstrating the development of relative grain size frequency with prolongation of sintering time in ceramics A_1 and B_1. At the beginning of isothermal sintering, the medium grain size in ceramics B_1 is equal to that in A_1. In compacts A_1 the grain size distribution is broader, and there are some bigger grains. These can result in abnormal grain growth in accordance with recognized tendencies.[5]

Table 1 contains the densities of the ceramics, the mean grain sizes and standard deviations for the grain size distribution. It can be seen that no density increase occurs for the sinter-active powder B with greater sintering time, whereas for the powder mixture A the density continues to increase. The faster sintering of B, concluded from dilatometry during heat up,[3] is confirmed. The presumption that the second phase regions were rich in sintering aid elements (for instance Pb), could not be confirmed. For example Fig. 3(e) for B_0 ceramics sintered to high density (97·3%), shows the secondary phase.

Quantitative image analysis with two alternative stereologic methods led to a value of 6 vol.% for the secondary phase in sintered compacts A_1, B_1 after 40 h. As Fig. 8 shows, the grain size of the mentioned

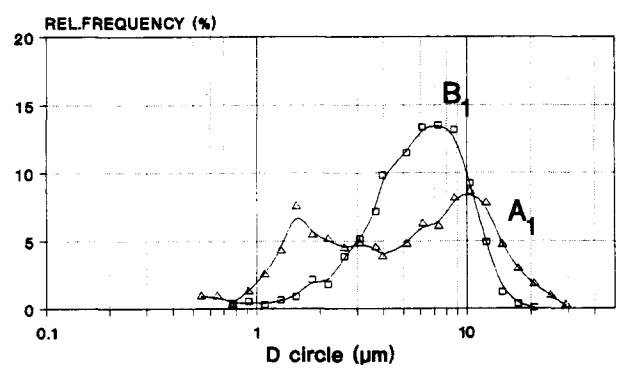

Fig. 5. Grain size distribution in A_1 and B_1 sintered at 1100°C for 40 h (see Figs 2(d) and 3(d)).

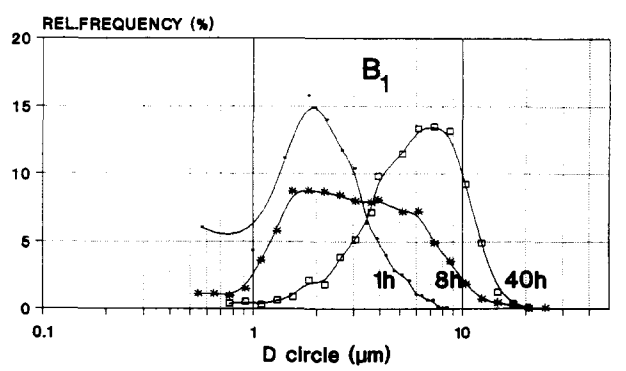

Fig. 7. Development of grain size distribution for ceramics B_1 sintered at 1100°C for 1 h, 8 h and 40 h (see Fig. 3(a), (c) and (d)).

Table 1. Grain size and grain size distribution in ceramics A and B sintered at 1100°C for 1, 4, 8 and 40 h

Sample	*Time (h)*	*Figure*	*Density (%)*	*Grain size (μm)*	
				Arithmetic mean	*Standard deviation*
A_1	1	2 (a)	95·6	2·54	1·71
	4	2 (b)	97·1	3·16	3·72
	8	2 (c)	97·2	4·65	4·07
	40	2 (d)	97·5	6·58	5·21
A_0	40	2 (e)	95·0	3·70	1·90
B_1	1	3 (a)	97·9	2·69	1·39
	4	3 (b)	97·6	3·56	2·14
	8	3 (c)	98·2	3·35	2·27
	40	3 (d)	97·8	6·40	2·99
B_0	40	3 (e)	97·3	4·90	2·10

phase in ceramics of powder B is smaller and more narrowly distributed than in ceramics of powder A. Table 2 lists the values.

To summarize the results of this section, powder B, consisting of metastable defect spinel particles, sinters faster than powder mixture A and leads to more homogeneous microstructure with normal grain size distribution.

4 Investigation of Phase Development

The drop-shaped secondary phase was investigated with SEM (BSE-contrast) and X-ray fluorescence analysis. The secondary phase is brighter than the matrix in the image of back-scattered electrons (Fig. 9).

This finding for elements with higher atomic number in the secondary phase was more thoroughly investigated with EDX-microprobe. Figure 10 shows typical EDX-spectra of the matrix and secondary phase after sintering at 1100°C for 40 h in O_2. It can be concluded that the secondary phase is richer in Ni. The determined amount of Mn can be

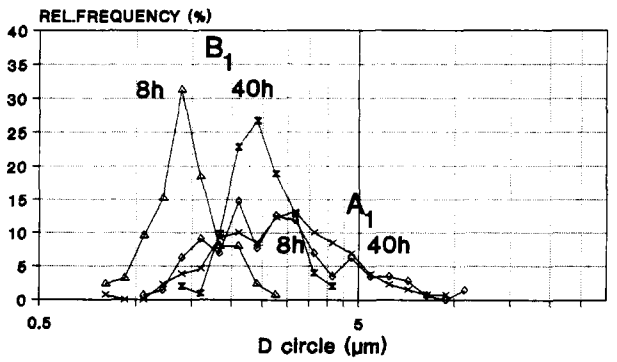

Fig. 8. Grain size distribution of the secondary phase in ceramics A_1 and B_1 sintered at 1100°C for 8 h and 40 h in oxygen (see Figs 2(c) and (d) and 3(c) and (d)).

Table 2. Secondary phase grain size, grain size distribution and volumetric share in ceramics sintered at 1100°C for 8 and 40 h

Sample	*Time (h)*	*Figure*	*Grain size (μm)*		*Volumetric share (%)*	
			Arithmetic mean	*Standard deviation*	*Square analysis*	*Linear analysis*
A_1	8	2 (c)	3·16	1·50	4·05	4·02
	40	2 (d)	3·12	1·73	5·94	5·95
B_1	8	3 (c)	1·67	0·41	3·80	3·82
	40	3 (d)	2·50	0·54	6·18	6·20

explained by the fact that the volume excited by the electron beam is larger than the investigated phase volume. In the surrounding matrix a higher Mn content is quantitatively detectable, which corresponds to the NiO separation. This leads to the conclusion that the upper temperature limit for $NiMn_2O_4$ stability published by Wickham[1] is not correct, and the decomposition of $NiMn_2O_4$ under formation of Mn-rich spinel and NiO separation, according eqn (1), begins at lower temperature:

$$NiMn_2^{III}O_4 \rightarrow xNiO + \frac{3-x}{3} Ni^{II}_{(3-3x)/(3-x)}Mn^{II}_{2x/(3-x)} Mn_2^{III}O_4 + \frac{x}{6}O_2 \quad (1)$$

The formula

$$Ni_{1-v}^{2+}Mn_v^{2+}[Ni_v^{2+}Mn_{2-2v}^{3+}Mn_v^{4+}]O_4$$

is used for understanding the electrical properties of the inverse spinel.[6] Thermogravimetric investigations (Netzsch STA 429) with 10 K/min and 2·5 K/min heating and cooling rate of the single-phase spinel, prepared by thermal treatment of $NiMn_2\square_{3\delta/4}O_{4+\delta}$ at 1000°C and 1 h annealing at 800°C, confirm that $NiMn_2O_4$ already decomposes under oxygen release at 975°C in oxygen and at 960°C in air.

Table 3 verifies that in tablets sintered at 1100°C oxygen deficits corresponding to eqn (1) appear, even after annealing at 800°C for 1 h. For porous samples B_0, reoxidation takes place in a shorter time and more completely than in compacts B_1 more

Table 3. Composition of ceramics, determined from the redox-equivalents, as a function of the sintering conditions

Sample	*Sintering conditions*	*Composition*
B_0	40 h, 1 100°C, O_2; 1 h, 800°C, O_2	$NiMn_2O_{4.00}$
B_1	40 h, 1 100°C, O_2; 1 h, 800°C, O_2	$NiMn_2O_{3.93}$
B_0	40 h, 1 100°C, O_2	$NiMn_2O_{3.93}$
B_0	40 h, 1 100°C, air; 1 h, 800°C, air	$NiMn_2O_{3.83}$
B_1	40 h, 1 000°C, O_2; 30 h, 800°C, O_2	$NiMn_2O_{3.99}$
B_0	40 h, 950°C, O_2; 1 h, 800°C, O_2	$NiMn_2O_{4.00}$
B_1	40 h, 950°C, O_2; 1 h, 800°C, O_2	$NiMn_2O_{4.01}$

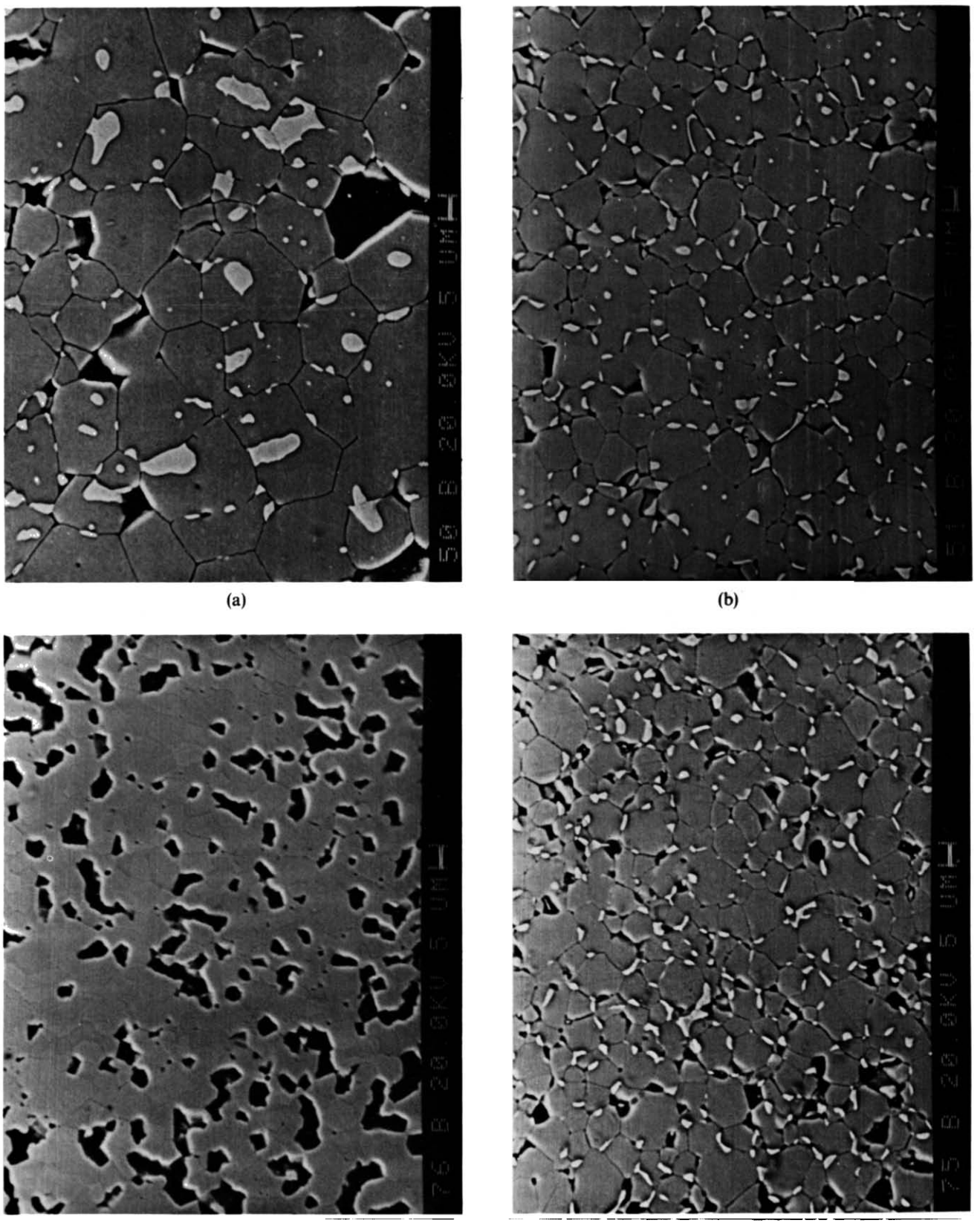

Fig. 9. SEM micrographs of ceramics sintered at 1100°C and annealed at 800°C for 1 h in oxygen: (a) A_1; (b) B_1; (c) B_0, density 86.7%; (d) B_0, density 97·7%.

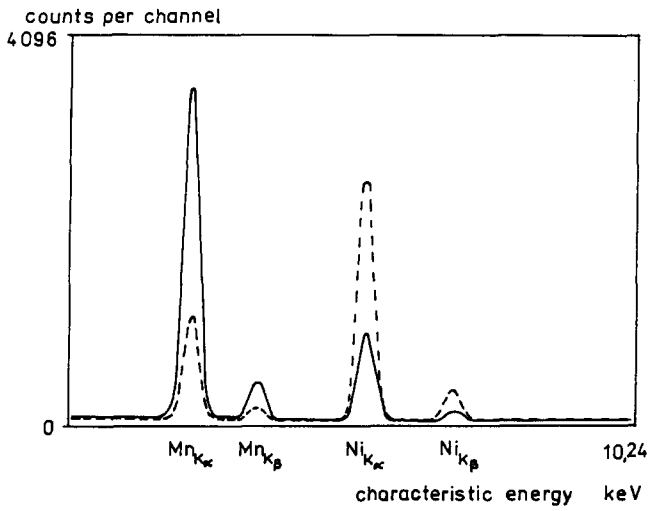

Fig. 10. EDX spectra of matrix (——) and secondary (– – –) phase in a sintered, decomposed spinel (see Fig. 9(a)).

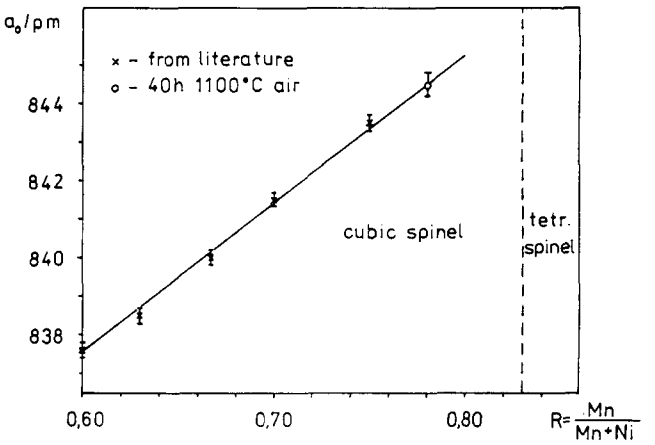

Fig. 11. Dependence of the lattice constant a_0 versus composition of the cubic spinel $Ni_x^{III}Mn_{1-x}^{II}Mn_2^{III}O_4$; literature values from Ref. 1.

densified by the sintering aid, or in compacts B_0 more densified by sintering in air. XRD shows only the pattern of the cubic spinel in all cases. The NiO pattern was not detectable. Only a little shift of the reflex positions can be observed.

The greatest NiO separation was determined in a sample sintered at 1100°C in air:

$$NiMn_2^{III}O_4 \rightarrow 0{\cdot}44NiO + 0{\cdot}85Ni_{0{\cdot}66}^{II}Mn_{0{\cdot}34}^{II}\,Mn_2^{III}O_4 + 0.07O_2 \quad (2)$$

The reaction product is determined by the analysis of the oxidation equivalents (see Table 3), which confirms the composition according to eqn (2), following from eqn (1) with $x = 0{\cdot}44$. The XRD pattern of this sample shows a shift of the reflections to smaller angles.

The lattice constant (a_0) of this cubic spinel is $844{\cdot}4 \pm 0{\cdot}5$ pm. The lattice constant of $NiMn_2O_4$ was determined to be $839{\cdot}9 \pm 0{\cdot}8$ pm, which is in good agreement with the published values.[7,8] The plot of the lattice constants versus composition of the cubic spinel $Ni_x^{II}Mn_{1-x}^{II}Mn_2^{III}O_4$ leads to the relationship shown in Fig. 11.

The substance of the composition with R = Mn/(Ni + Mn) = 0·78, equivalent to the spinel composition $Ni_{0{\cdot}66}^{II}Mn_{0{\cdot}34}^{II}Mn_2^{III}O_4$ and with $a_0 = 844{\cdot}4$ pm, was obtained by sintering a 1100°C in air. Figure 12 shows the confirming TG results. It can be seen that only in the case of porous compacts B_0 the weight loss from oxygen release above 975°C can be compensated by reoxidation during cooling (see Fig. 9(c)). A sample B_0 (Fig. 9(d)), sintered at 1100°C in O_2 to high density (97·3%), cannot be

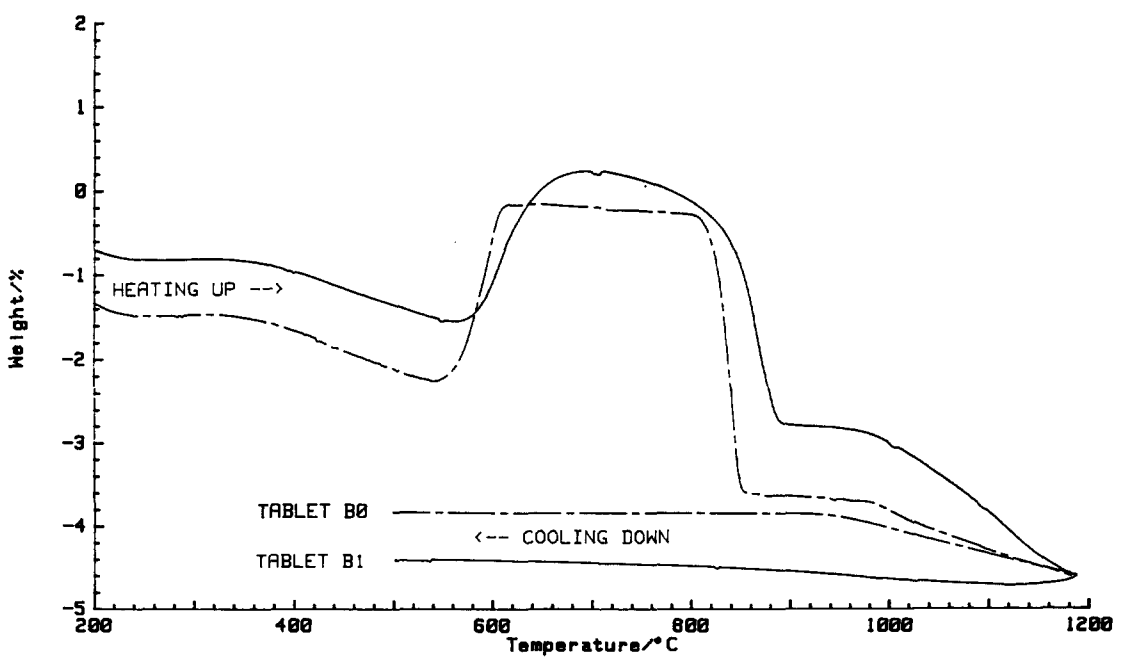

Fig. 12. Thermogravimetry of tablets B_0 and B_1 (50 m^2/g) in oxygen; sample weight, 90 mg; heating and cooling rate, 10 K/min.

Table 4. Density of ceramics B_1 as a function of sintering temperature and atmosphere.

Temperature (°C)	*Density* (%)	
	Air	*Oxygen*
900	91·2	—
950	—	94·0
1 000	98·3	96·8
1 100	99·4	97·7

reoxidized to $NiMn_2O_4$ by annealing for 1 h at 800°C.

Dense ceramics B_1 sintered above 975°C in O_2 to obtain high density, can be nearly completely reoxidized by extreme prolongation of the annealing time to 30 or more hours. The necessary time depends on the sample size. These results for $NiMn_2O_4$ spinel decomposition are in good agreement with those by Macklen,[9] who investigated the dependence of oxygen release on the temperature and oxygen partial pressure by isothermal thermogravimetry. He found the composition $NiMn_2O_{3.927}$ for 1095°C in oxygen.

5 The Importance of the Spinel Decomposition for Dense Sintering

The sinter densities in Table 4 prove that isothermal sintering in air under the same conditions of temperature and time leads to higher densities than in oxygen. If the sintering temperature is kept below 975°C (the temperature of decomposition), densities larger than 95% cannot be obtained, not even by much longer sintering time. Only sintering under higher temperatures (1000°C for instance) makes possible densities larger than 95%. The spinel decomposition above 975°C induces lattice mobility and hence diffusion processes, leading to grain growth by further elimination of closed pores.

6 Summary

The decomposition of the spinel starts at 960°C in air and at 975°C in oxygen. In this process NiO separation in a Mn-rich spinel matrix phase $Ni_x^{II}Mn_{1-x}^{II}Mn_2^{III}O_4$ occurs with oxygen loss. The two-phase composition of ceramics of both A and B powders after sintering at temperatures above 1000°C was proved by means of the EDX-microprobe, determination of oxidation equivalent and lattice constant changes. Annealing at temperatures in the stability region of the spinel (800°C for instance) permitted the reoxidation to a one-phase spinel if high sinter density was obtained.

Therefore, the sinter-active powder B with a maximum of the shrinkage rate at 950°C[3] offers the precondition for an optimized sintering schedule leading to single-phase $NiMn_2O_4$ semiconductor ceramics. The alternative route to $NiMn_2O_4$ ceramics of high density with homogeneous microstructure involves first stimulation of sintering by spinel decomposition with NiO separation and oxygen release and secondly reoxidation in the stability region of the spinel.

References

1. Wickham, D. G., Solid-phase equilibria in the system NiO-MN_2O_3-O_2. *J. Inorg. Nucl. Chem.*, **26** (1964) 1360.
2. Feltz, A. & Töpfer, J., Bildung von Defektspinellen und Phasenbeziehungen im System $Ni_xMn_{3-x}O_4$. *Z. anorg. allg. Chem.*, **576** (1989) 71–80.
3. Jung, J., Töpfer, J., Feltz, A., Körner, U., Schirrmeister, F., Bühling, D., Kuzelka, K.-H., & Röder, G., Thermoanalytic characterization of $NiMn_2O_4$ formation. *J. Thermal Analysis* (in press).
4. Feltz, A. *et al.*, Verfahren zur Herstellung einer Sinterkeramik für hochgenaue Thermistoren. German Patent WP-DD 3 193 924, 1 September 1988.
5. Kingery, W. D., *Introduction to Ceramics*. John Wiley and Sons, New York, 1976, pp. 448–583.
6. Xiao-Xia Tang, Matthiram, A. & Goodenough, J. B., $NiMn_2O_4$ revisited. *J. Less Common Metals*, **156** (1989) 357–68.
7. Larson, E. G., Arnot, R. J. & Wickham, D. G., Preparation, semiconduction and low-temperature magnetization of the system $Ni_{1-x}Mn_{2-x}O_4$. *J. Phys. Chem. Solid*, **23** (1962) 1771–81.
8. Boucher, B., Buhl, R. & Perrin, M., Etude cristallographique du manganite spinelle cubique $NiMn_2O_4$. *Acta Cryst.*, **B25** (1969) 2326.
9. Macklen, E. D., Electric conductivity and cation distribution in nickel manganite. *J. Phys. Chem. Solids*, **47**(11) (1986) 1073–9.